Comput. Math. Applic. Vol. 16, No. 1/2, pp. 57–68, 1988
Printed in Great Britain.

0097-4943/88 $3.00 + 0.00

APPLICATIONS OF THE FINITE ELEMENT METHOD TO MODELING THE ATMOSPHERIC BOUNDARY LAYER

E. S. TAKLE[1] and R. D. RUSSELL[2]

[1]Departments of Agronomy and Earth Science, Iowa State University, Ames, IA 50011, U.S.A.

[2]Physical Science Department, Auburn University at Montgomery, Montgomery, AL 36193, U.S.A.

Abstract—The finite element method is used to describe the detailed properties of the atmospheric boundary layer by use of a high-resolution model and its bulk properties by use of a simple vertically integrated model. Features of the finite element method that can be exploited for applications to the atmospheric boundary layer include the capability to use different basis functions in different parts of the domain, ability to grid over irregular terrain, ease of using time-dependent basis functions and the natural way that surface boundary conditions and vertically integrated properties enter the model.

1. INTRODUCTION

The atmospheric boundary layer is that part of the atmosphere that is directly influenced by the turbulence generated by thermal and mechanical interaction with the earth's surface. The depth of this boundary layer varies from about a 100 m under stable, nighttime conditions to over 3 km under highly convective daytime conditions at low latitudes. Above this region, stress on the flow arising from the fluid interactions with the surface is assumed to be negligible.

The atmospheric boundary layer is where we live, raise our crops, dispose of our air pollutants, put up our windmills, land our airplanes, build our buildings, beam our electromagnetic communication signals and carry on a host of other activities that are influenced by the mean and turbulent properties of the fluid environment. Furthermore, the boundary layer is the gateway for interchange of heat, momentum, moisture and trace gases between the surface and the rest of the atmosphere. Improved understanding of the atmospheric boundary layer may be a key to extending the general predictability of the atmosphere by replacing some of the dependence on initial conditions with dependence on boundary conditions, thereby reducing the accuracy degradation of the initial-value problem.

We have used the finite element method to produce numerical solutions to the boundary-layer equations for several flows of interest. In Section 2, we present the basic equations for a high-resolution model of the atmospheric boundary layer, their formulation in the finite element representation and some applications we have made to one- and two-dimensional problems of interest in boundary-layer meteorology. In Section 3 we describe a vertically integrated model cast in the Galerkin finite element method and an application to the stable boundary layer.

2. HIGH-RESOLUTION MODEL

We have developed a high-resolution atmospheric boundary-layer model for application to problems requiring detailed knowledge of the structure of the mean and turbulent flow near the earth. The basic model we use is an extension of the two-dimensional finite element model developed by Chan *et al.* [1]. We represent the mean two-dimensional (vertical and one horizontal) fluid properties of the dry atmospheric boundary layer by the hydrostatic, incompressible Boussinesq equations, which are applicable to a fluid experiencing shallow convection with vertical scales of motion about an order of magnitude less than horizontal scales. A brief outline of the model and its representation in the finite element formulation is presented below.

Governing Equations

The fluid velocity components are represented by u, v and w (w being the vertical velocity), θ is the potential temperature, and π is the Exner pressure function. Values of θ and π are related to measured temperature (T) and pressure (p) by the following:

$$\theta = T\left(\frac{p_0}{p}\right)^{R_d/c_{pd}} \text{ and } \quad \pi = c_p\left(\frac{p}{p_0}\right)^{R_d/c_{pd}},$$

where p_0 is the surface reference pressure, R_d is the specific gas constant for dry air and c_{pd} is the specific heat capacity at constant pressure for dry air. The potential temperature and Exner function are decomposed into a steady, basic-state component (denoted by subscript zero) and a deviation (denoted by a prime):

$$\theta = \theta_0 + \theta' \quad \text{and} \quad \pi = \pi_0 + \pi'.$$

Velocity components are considered to have grid-volume mean values denoted by an over bar. The basic equations are then [2]:

$$\frac{\partial \bar{u}}{\partial t} = -\bar{u}\frac{\partial \bar{u}}{\partial x} - \bar{w}\frac{\partial \bar{u}}{\partial z} - \theta_0\frac{\partial \overline{\pi'}}{\partial x} + \frac{\partial}{\partial x}\left(K_x^m\frac{\partial \bar{u}}{\partial x}\right) + \frac{\partial}{\partial z}\left(K_z^m\frac{\partial \bar{u}}{\partial z}\right) + f(\bar{v} - v_g), \tag{1}$$

$$\frac{\partial \bar{v}}{\partial t} = -\bar{u}\frac{\partial \bar{v}}{\partial x} - \bar{w}\frac{\partial \bar{v}}{\partial z} + \frac{\partial}{\partial x}\left(K_x^m\frac{\partial \bar{v}}{\partial x}\right) + \frac{\partial}{\partial z}\left(K_z^m\frac{\partial \bar{v}}{\partial z}\right) + f(u_g - \bar{u}), \tag{2}$$

$$\frac{\partial \overline{\pi'}}{\partial z} = \frac{\overline{\theta'}}{\theta_0^2}g_0, \tag{3}$$

$$\frac{\partial \bar{u}}{\partial x} + \frac{\partial \bar{w}}{\partial z} = 0 \tag{4}$$

and

$$\frac{\partial \overline{\theta'}}{\partial t} = -u\frac{\partial \overline{\theta'}}{\partial x} - w\frac{\partial \overline{\theta'}}{\partial z} + \frac{\partial}{\partial x}\left(K_x^h\frac{\partial \overline{\theta'}}{\partial x}\right) + \frac{\partial}{\partial z}\left(K_z^h\frac{\partial \overline{\theta'}}{\partial z}\right). \tag{5}$$

The acceleration due to gravity is given by g_0, and the large-scale pressure gradient term is replaced by the geostrophic-wind approximation (u_g, v_g). We have used the gradient transfer approximation to represent the dominant Reynold's stress terms. The vertical turbulent exchange coefficients, K_z, for momentum (K_z^m) and heat (K_z^h) are determined by the Kolmogorov equation, $K = c\bar{E}^{1/2}l$ [3], where $\bar{E}$ is the turbulence kinetic energy and l is a characteristic length scale determined diagnostically by the method of Therry and Lacarrere [4]. We use a value of 0.52 for c. The equation for $\bar{E}$ is

$$\frac{\partial \bar{E}}{\partial t} = -\bar{u}\frac{\partial \bar{E}}{\partial x} - \bar{w}\frac{\partial \bar{E}}{\partial z} + \frac{\partial}{\partial x}\left(K_x^m\frac{\partial \bar{E}}{\partial x}\right) + \frac{\partial}{\partial z}\left(K_z^m\frac{\partial \bar{E}}{\partial z}\right) + K_z^m\left[\left(\frac{\partial \bar{u}}{\partial z}\right) + \left(\frac{\partial \bar{v}}{\partial z}\right)^2\right] - K_z^h\frac{g_0}{\theta_0}\frac{\partial \overline{\theta'}}{\partial z} - a\bar{E}^{3/2}/l, \tag{6}$$

where $a = 0.14$. The last three terms represent, respectively, generation of $\bar{E}$ by shear production, generation by buoyancy and dissipation. Transport by pressure velocity correlations are parameterized by diffusion. The K_x diffusion terms in equations (1), (2), (5) and (6) represent horizontal smoothing, and have little physical basis.

Finite Element Representation

The finite element method is used to approximate the solution to the governing differential equations by use of the following expansions:

$$\bar{q}(t, x, z) \approx \tilde{q}(t, x, z) \equiv \sum_{i=1}^{9} \hat{q}_i(t)\Psi_i(x, z) \tag{7}$$

and

$$\tilde{\pi}'(t, x, z) \approx \tilde{\pi}(t, x, z) \equiv \sum_{i=1}^{4} \hat{\pi}(t)\phi_i(x, z), \tag{8}$$

where q represents any of the five dependent variables u, v, w, θ' or E; Ψs represent the nine-node biquadratic shape functions; and ϕs represent the shape functions for pressure, which may be either bilinear ($i = 1, \ldots, 4$) or biquadratic ($i = 1, \ldots, 9$). The Galerkin method is applied to the prognostic equations and the least-squares method is applied to the diagnostic equations. We substitute equations (7) and (8) into equations (1)–(5), multiply by the appropriate shape function as weight, and integrate over the element domain, Ω_e, to obtain the following equations [5]:

$$\sum_{i=1}^{9}\left[\frac{\mathrm{d}\hat{u}_i}{\mathrm{d}t}\iint_{\Omega_e}\Psi_i\Psi_j\,\mathrm{d}A + \hat{u}_i\iint_{\Omega_e}\left(u\Psi_j\frac{\partial\Psi_i}{\partial x} + w\Psi_j\frac{\partial\Psi_i}{\partial z} + K_x^{\mathrm{m}}\frac{\partial\Psi_i}{\partial x}\frac{\partial\Psi_j}{\partial x} + K_z^{\mathrm{m}}\frac{\partial\Psi_i}{\partial z}\frac{\partial\Psi_j}{\partial z}\right)\mathrm{d}A\right]$$

$$= \sum_{i=1}^{9}\iint_{\Omega_e}\hat{v}_i\Psi_i f\Psi_j\,\mathrm{d}A + \int_{\Gamma_e^1}\Psi_j\left(K_x^{\mathrm{m}}\frac{\partial u}{\partial x}n_x + K_z^{\mathrm{m}}\frac{\partial u}{\partial z}n_z\right)\mathrm{d}l$$

$$- \sum_{k=1}^{4}\theta_0\hat{\pi}_k'\iint_{\Omega_e}\Psi_j\frac{\partial\phi_k}{\partial x}\,\mathrm{d}A - \iint_{\Omega_e}fv_{\mathrm{g}}\Psi_j\,\mathrm{d}A \quad (j = 1,2,\ldots,9), \tag{9}$$

$$\sum_{i=1}^{9}\left[\frac{\mathrm{d}\hat{v}_i}{\mathrm{d}t}\iint_{\Omega_e}\Psi_i\Psi_j\,\mathrm{d}A + \hat{v}_i\iint_{\Omega_e}\left(u\Psi_j\frac{\partial\Psi_i}{\partial x} + w\Psi_j\frac{\partial\Psi_i}{\partial z} + K_x^{\mathrm{m}}\frac{\partial\Psi_i}{\partial x}\frac{\partial\Psi_j}{\partial x} + K_z^{\mathrm{m}}\frac{\partial\Psi_i}{\partial z}\frac{\partial\Psi_j}{\partial z}\right)\mathrm{d}A\right]$$

$$= -\sum_{i=1}^{9}\iint_{\Omega_e}\hat{u}_i\Psi_i f\Psi_j\,\mathrm{d}A + \int_{\Gamma_e^1}\Psi_j\left(K_x^{\mathrm{m}}\frac{\partial v}{\partial x}n_x + K_z^{\mathrm{m}}\frac{\partial v}{\partial z}n_z\right)\mathrm{d}l$$

$$+ \iint_{\Omega_e}fu_{\mathrm{g}}\Psi_j\,\mathrm{d}A \quad (j = 1, 2, \ldots, 9), \tag{10}$$

$$\sum_{i=1}^{4}\hat{\pi}_i'\iint_{\Omega_e}\frac{\partial\phi_i}{\partial z}\frac{\partial\phi_j}{\partial z}\,\mathrm{d}A = \sum_{k=1}^{9}\frac{1}{\theta_0^2}g_0\hat{\theta}_k'\iint_{\Omega_e}\frac{\partial\phi_j}{\partial z}\Psi_k\,\mathrm{d}A \quad (j = 1, 2, 3, 4), \tag{11}$$

$$\sum_{i=1}^{9}\hat{w}_i\iint_{\Omega_e}\frac{\partial\Psi_j}{\partial z}\frac{\partial\Psi_i}{\partial z}\,\mathrm{d}A = -\sum_{k=1}^{9}\hat{u}_k\iint_{\Omega_e}\frac{\partial\Psi_j}{\partial z}\frac{\partial\Psi_k}{\partial x}\,\mathrm{d}A \quad (j = 1, 2, \ldots, 9) \tag{12}$$

and

$$\sum_{i=1}^{9}\left[\frac{\mathrm{d}\hat{\theta}_i}{\mathrm{d}t}\iint_{\Omega_e}\Psi_i\Psi_j\,\mathrm{d}A + \hat{\theta}_i'\iint_{\Omega_e}\left(u\Psi_j\frac{\partial\Psi_i}{\partial x} + w\Psi_j\frac{\partial\Psi_i}{\partial z} + K_x^{\mathrm{h}}\frac{\partial\Psi_i}{\partial x}\frac{\partial\Psi_j}{\partial x} + K_z^{\mathrm{h}}\frac{\partial\Psi_i}{\partial z}\frac{\partial\Psi_j}{\partial z}\right)\mathrm{d}A\right]$$

$$= \int_{\Gamma_e^2}\Psi_j\left(K_x^{\mathrm{h}}\frac{\partial\theta'}{\partial x}n_x + K_z^{\mathrm{h}}\frac{\partial\theta'}{\partial z}n_z\right)\mathrm{d}l \quad (j = 1, 2, \ldots, 9). \tag{13}$$

Green's theorem has been used on the diffusion terms to eliminate the second derivative. In the nonlinear terms, the advection speeds (unsubscripted u and w) in equations (9), (10) and (13) are taken as the values from the previous time step. The boundaries of the element domain, Ω_e, are given by Γ_e^1 and Γ_e^2, which represent, respectively, those portions of the boundary of the element on which the momentum fluxes

$$\left[K_x^{\mathrm{m}}\frac{\partial u}{\partial x}, K_z^{\mathrm{m}}\frac{\partial u}{\partial z} \quad \text{in equation (9)} \quad \text{and} \quad K_x^{\mathrm{m}}\frac{\partial v}{\partial x}, K_z^{\mathrm{m}}\frac{\partial v}{\partial z} \quad \text{in equation (10)}\right]$$

and heat fluxes

$$\left[K_x^{\mathrm{h}}\frac{\partial\theta'}{\partial x} \quad \text{and} \quad K_z^{\mathrm{h}}\frac{\partial\theta'}{\partial z} \quad \text{in equation (13)}\right]$$

are specified. The equation for E is solved by the method of fractional steps, as described by Mailhot and Benoit [6], in which we first neglect advection and diffusion and find an intermediate value from

$$\frac{\partial \bar{E}}{\partial t} = P\bar{E}^{1/2} - D\bar{E}^{3/2}, \tag{14}$$

where P is the coefficient of the production term and D is the coefficient of the dissipation term [3]. We then solve the equation

$$\frac{\partial \bar{E}}{\partial t} = -u\frac{\partial \bar{E}}{\partial x} - w\frac{\partial \bar{E}}{\partial z} + \frac{\partial}{\partial x}\left(K_x^m \frac{\partial \bar{E}}{\partial x}\right) + \frac{\partial}{\partial z}\left(K_z^m \frac{\partial \bar{E}}{\partial z}\right) \tag{15}$$

by use of the finite element method for the final value of $\bar{E}$, which gives

$$\sum_{i=1}^{9}\left[\frac{d\hat{E}_i}{dt}\iint_{\Omega_e}\Psi_i\Psi_j\,dA + \hat{E}_i\iint_{\Omega_e}\left(u\Psi_j\frac{\partial\Psi_i}{\partial x} + w\Psi_j\frac{\partial\Psi_i}{\partial z} + K_x^m\frac{\partial\Psi_j}{\partial x}\frac{\partial\Psi_i}{\partial x} + K_z^m\frac{\partial\Psi_j}{\partial z}\frac{\partial\Psi_i}{\partial z}\right)dA\right]$$

$$= \int_{\Gamma_e^3}\Psi_j\left(K_x^m\frac{\partial\bar{E}}{\partial x}n_x + K_z^m\frac{\partial\bar{E}}{\partial z}n_z\right)dl \quad (j = 1, 2, \ldots, 9), \tag{16}$$

where Γ_e^3 is that portion of the boundary of element e where the normal derivative of E is specified. A modified Crank–Nicholson scheme is used to convert the ordinary differential equations in time to algebraic equations [5].

Applications

Stratified flow

The model has been applied to both unstable and stably stratified flow in the atmospheric boundary layer. A summary of past reports and some recent results shows the versatility of the model.

Unstable flow—the sea breeze. We have applied the finite element model to the time-dependent sea-breeze circulation. The domain consists of 105 nine-node elements (465 total nodes) covering a domain 89 km in the horizontal direction perpendicular to the coast and 2 km in the vertical. Nodal spacing in the vertical ranges from 4 m near the surface to 300 m near the top of the domain. In the horizontal direction, nodal spacing is 2.5 km near the shore and 4 km at the domain boundary. We specify a surface roughness (z_0) of 0.05 m over the land and 0.015 m over the sea. The initial wind field is driven from the top by a 2.5 m/s geostrophic wind in the off-shore direction. The initial temperature field is neutral from the surface to 160 m and stable ($d\theta/dz = 0.0076$ K/m) from 160 to 2000 m. We simulate heating over the land by specifying the surface temperature to have a sinusoidal time dependence, increasing from zero at $t = 0$ to a maximum amplitude of 10°C at $t = 6$ h. The surface temperature over the water is held constant in time.

A sample of the results is shown in Fig. 1, where the wind field 5 h after sunrise is presented. The heating over the land has produced an increase in temperature that results in a maximum pressure gradient at the shore. At the time shown, the gradient has increased to the point that the initial left-to-right flow has been reversed immediately off-shore, creating on-shore flow and a sea-breeze front 7 km inland. The updraft maximum is located 2.5 km from the shore at about 350 m above the surface and has a value in excess of 10 cm/s. These results show somewhat weaker on-shore flow than the earlier simulations of Chang *et al.* [5] who used a simpler turbulence scheme; but both simulations agree with our general understanding of the sea-breeze circulation.

Stable flow—the nocturnal boundary layer. A simulation was made of the horizontally homogeneous atmospheric boundary layer under conditions of constant nighttime surface cooling of 1°C/h. The initial conditions consisted of a neutral temperature profile and a wind field driven by a 10 m/s wind at the top (1500 m). As shown in Fig. 2, the model develops a nocturnal jet at 85 m after about 6 h of cooling. Such a jet is frequently observed in the nocturnal boundary layer [7]. The height of the jet maximum, its development through the nighttime period and its maximum speed are dependent on large-scale conditions and the surface cooling rate. However, its general features are represented quite well by the model.

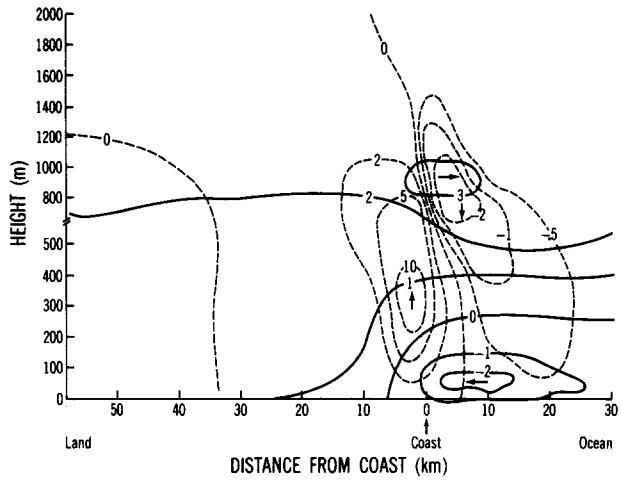

Fig. 1. Model results of the sea-breeze flow field 5 h after the onset of surface heating. An off-shore geostrophic wind of 2.5 m/s is assumed. Contours of horizontal velocity are given in m/s and contours of vertical velocity are given in cm/s.

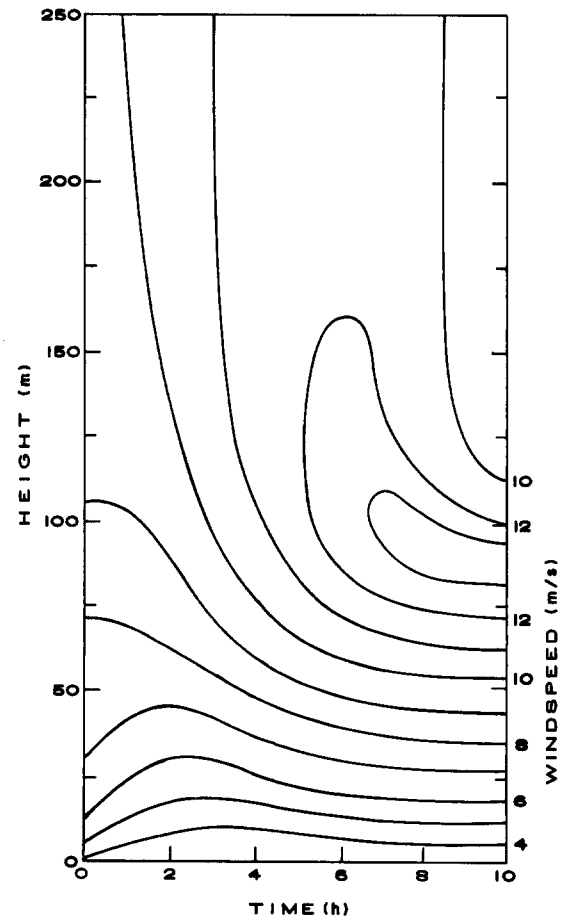

Fig. 2. Model results of the evolution of the wind speed in the stable boundary layer with a surface cooling rate of 1°C/h applied starting at $t = 0$.

Table 1. Parameters describing the stable boundary layer at steady state for a 1°C/h surface cooling rate as reported by Wyngaard [8], Brost and Wyngaard [9], Zeman [10] and Russell and Takle [3] and as obtained from the finite element vertically integrated (FEVI) model

Parameter	Ref. [8]	Ref. [9]	Ref. [10]	Ref. [3]	FEVI
u_*(m/s)	0.16	0.18	0.19	0.185	0.17
Q_0(K m/s)	−0.016	−0.020	−0.019	−0.0189	−0.015
L(m)	25	25	28	28	27
α(deg)	44	38	40	40	40
h(m)	48	85	98	89	73
d^*	0.24	0.40	0.42	0.39	0.34
h/L	2.0	3.4	3.5	3.2	2.7
u_*/fL	67	74	66	68	63

Our model results are consistent with the results of other numerical models of the cooling boundary layer, as shown in Table 1 [8–10]. The model results compared in Table 1 are, respectively, the friction velocity, surface heat flux, Monin–Obukhov stability parameter, angular difference between the wind direction at the top and bottom of the boundary layer, height of the boundary layer and three boundary-layer parameters defined in terms of model-derived values [8]. The model of Wyngaard [8] is the most physically complete of those listed. The results of the model of Zeman [10] and those from the finite element integrated model are discussed in Section 3.

Flow over irregular boundaries

Flow over irregular boundaries creates the need for irregular grids and for accurate representation of the effects of dynamic pressure caused by changes in roughness and interaction of the flow with the terrain. By use of isoparametric elements, we grid over irregular terrain and concentrate nodes in regions of large gradients. We have extended the procedure of Song *et al.* [11] for parameterizing nonhydrostatic terrain effects into our model. We have compared our model results with observations for flow over a low hill at a coastal site, as reported by Peterson *et al.* [12]. The results are shown in Figs 3a–3d.

Figure 3a is a schematic diagram showing the locations of three 12-m masts having instruments at 1-, 2-, 3-, 5-, 8- and 12-m levels. The masts are located at distances of 10, 63, and 100 m from the shore. On-shore flow encounters an estimated roughness change from 0.01 to 1.0 cm.

Measurements of horizontal wind speed taken on 17 October 1974 under near-neutral conditions are shown in Fig. 3b. Notable features of these profiles are that the low-level flow experiences a decrease in speed due to the increased roughness. At the upper levels, the speed is increased due to the increase in terrain elevation. This causes the profiles from downwind masts to cross the profile of mast 1: profile B crosses at 3 m and profile C crosses between 6 and 7 m.

The results from a hydrostatic model simulation of this flow are shown in Fig. 3c. The reduction in speed at masts 2 and 3 is correctly simulated at low levels. However, the profiles do not cross, so the dynamic pressure effect of the hill is not simulated by the model. The results from the quasi-nonhydrostatic model, shown in Fig. 3d, demonstrate that this model does incorporate the dynamic effect of the rise in terrain and increase in height of the internal boundary layer away from the shore. In these results, profile B crosses A at about 2 m and profile C crosses A between 5 and 6 m. These preliminary results suggest that, although the model may benefit from additional refinements, it does have the correct physical mechanism to account for the dynamical effect of terrain on the flow.

Log-linear element

Cross-stream gradients of streamwise velocity become large near the boundary for fluid flow over a rigid surface. Accurate representation of the flow in these regions requires either a special wall layer of assumed analytical solutions or extremely fine resolution of the grid. Takle and Leone [13] constructed a long-linear element for use near the surface in atmospheric boundary-layer flows to more accurately simulate the known functional form of the velocity and temperature profiles in this region. The element contained nine nodes with quadratic dependence in the streamwise direction and log-linear dependence in the cross-stream direction. The log-linear function, being a monotonically increasing function away from the boundary, eliminates the poor representation near the top of the boundary element arising for quadratic functions, but yet gives much more

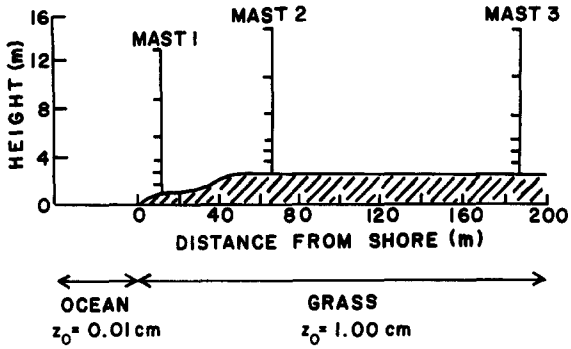

Fig. 3a. Schematic representation of the terrain and mast locations for comparison with the results of the quasi-nonhydrostatic model.

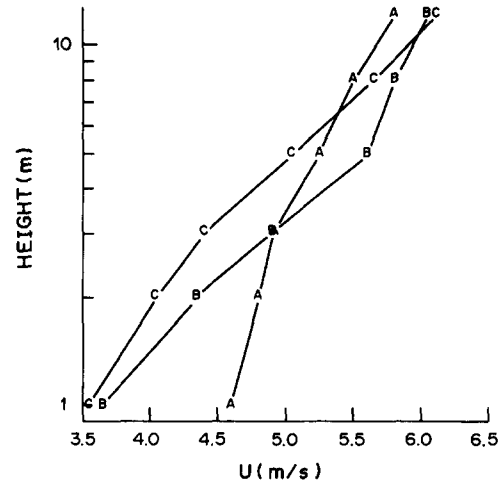

Fig. 3b. Observations of wind-speed profiles [12] under neutral on-shore flow at mast 1 (profile A), mast 2 (profile B) and mast 3 (profile C).

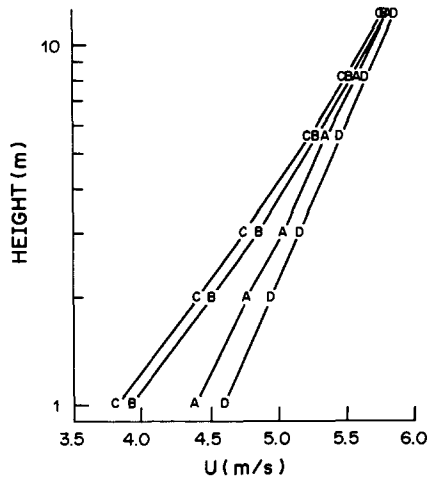

Fig. 3c. Wind-speed profile results from a hydrostatic model. Profile D is for the model upwind boundary taken to be 109 m seaward of the shore.

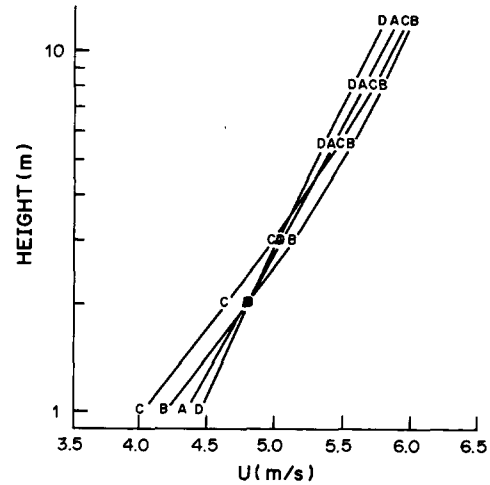

Fig. 3d. Wind-speed profile results from the quasi-nonhydrostatic model.

realistic gradients near the surface than linear basis functions. Applications to neutral and stably stratified atmospheric boundary layers showed that the number of nodes could be reduced by a factor of 2 by use of the log-linear element for neutral flow with no loss of accuracy. Furthermore, the coarser resolution permitted much larger timesteps to be taken [14]. For nonneutral flow, both velocity and temperature profiles were simulated very well by the log-linear element, although temperature was somewhat less accurately represented than velocity.

Moving finite element method

The moving finite element method was introduced by Miller and Miller [15] to allow computational nodes to migrate to regions of large gradient, thereby minimizing the total number of computational nodes required for a numerical solution of given accuracy. Gelinas *et al.* [16] and more recent works [17, 18] have expanded the theoretical framework for the moving finite element method.

The atmospheric boundary layer can, under certain conditions, develop regions of large gradients near the earth's surface or in the vicinity of the base of the warm, dry layer that frequently caps the atmospheric boundary layer over water (e.g. off the California coast). Kim [19] developed a moving finite element model from a fixed finite element code that solved equations (1)–(6). This problem is significantly more difficult than previous studies that used the moving finite element method because of the need to solve four equations [equations (1), (2), (5) and (6)] simultaneously, as opposed to the report of Gelinas *et al.* [16] wherein a single equation was solved. Any of the four equations may develop regions of large gradients, and not all in the same regions, so the migration of nodes is much more complex. Kim found the solution was subject to a rather complicated instability long after model initialization. A variable timestep and the use of regularization terms to prevent singularities in the mass matrix allowed for stable solutions out of 3 h of simulated time, but solutions did not compare well with other model results or observations. The use of weight functions to force nodal position to depend primarily on one variable was suggested but not tested. This topic needs more research. Potential applications include movement of the sea-breeze frontal zone or movement associated with large-scale air-mass boundaries, with their accompanied unsettled weather. A simpler application that uses time-dependent basis functions is described in the following section.

3. VERTICALLY INTEGRATED MODEL

Hemispheric- or global-scale prediction models of the entire atmosphere rarely can accommodate such a large number of nodes in the boundary layer as described in the model of Section 2. For such application, the effect on the overlying atmosphere, rather than internal details of the boundary layer, are of primary interest. To address this need, bulk models or vertically integrated models that use finite difference techniques have been suggested [7, 10, 20, 21]. Such models are one-dimensional models that describe the dynamic and thermodynamic coupling of the earth's surface to the free atmosphere through properties such as those listed in Table 1.

The daytime boundary layer is particularly well-described by a bulk model because of its relatively uniform vertical structure. The nighttime boundary layer, however, as pointed out by Zeman [10], is dominated by production of turbulence by vertical shear of the mean horizontal wind and suppression of turbulence by negative buoyancy. Accurate representation of the nocturnal boundary layer therefore requires gradients as well as mean values. The finite element method, being inherently an integral method, has advantages for this application.

Model Equations

We model the vertical structure of the nocturnal boundary layer with a finite element domain consisting of two elements and three nodes as shown in Fig. 4. The lower element is based at the top of the surface layer ($z = h_s$) and extends to the top of the boundary layer, $z = h(t)$. The top element represents the free atmosphere above the boundary layer. The size of the lower element is allowed to vary in time according to the physical processes within the boundary layer.

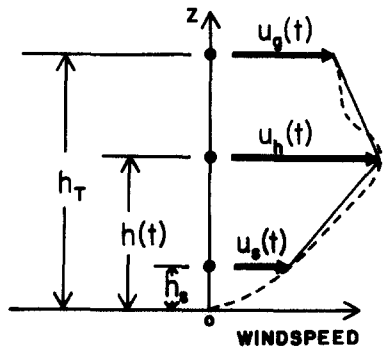

Fig. 4. Domain for the vertially integrated model.

Table 2. Variables and parameters in the basic equations for the vertically integrated model

q	Q^q	K^q
u	$f(v-v_g)$	K^m
v	$-f(u-u_g)$	K^m
θ	0	K^h

The one-dimensional, horizontally homogeneous equations describing the boundary layer are of the form (see Table 2)

$$\frac{\partial \bar{q}}{\partial t} = Q + \frac{\partial}{\partial z}\left(K^q \frac{\partial \bar{q}}{\partial z}\right). \tag{17}$$

To accommodate a boundary layer that deepens through the night, we expand the unknown variables in terms of linear basis functions, ϕ, which depend on both z and t, and for each element are given by

$$q(t, z) = \sum_{i=1}^{2} \hat{q}_i(t)\phi_i(t, z). \tag{18}$$

By substituting this into the model equations, we obtain

$$\sum_{i=1}^{2}\left\{\dot{\hat{q}}_i\phi_i + \hat{q}_i\dot{\phi}_i - \hat{q}_i\frac{\partial}{\partial z}\left(K^q\frac{\partial \phi_i}{\partial z}\right) - Q_i^q\phi_i\right\} = R^q, \tag{19}$$

where R^q is a small residual. Minimization of R^q with respect to the basis functions over the model domain according to the Galerkin procedure,

$$\int_{\Omega_e} \phi_j R^q \, dz = 0, \tag{20}$$

renders the model equations into the form

$$\sum_{i=1}^{2}\left\{\dot{\hat{q}}_i\int_{\Omega_e}\phi_j\phi_i\,dz + \hat{q}_i\int_{\Omega_e}\phi_j\dot{\phi}_i\,dz - \hat{q}_i\int_{\Omega_e}\phi_j\frac{\partial}{\partial z}\left(K^q\frac{\partial\phi_i}{\partial z}\right)dz - \int_{\Omega_e}\phi_j Q_i^q\phi_i\,dz\right\} = 0, \tag{21}$$

where $\dot{\phi}_i = \partial\phi_i/\partial t$. The diffusion term can be integrated by parts to give

$$-\sum_{i=1}^{2}\hat{q}_i\int_{\Omega_e}\phi_j\frac{\partial}{\partial z}\left(K^q\frac{\partial\phi_i}{\partial z}\right)dz = \sum_{i=1}^{2}\hat{q}_i\left\{\phi_j K^q\frac{\partial\phi_i}{\partial z}\bigg|_{\Gamma_e^q} + \frac{\partial\phi_j}{\partial z}\frac{\partial\phi_i}{\partial z}\int_{\Omega_e}K^q\,dz\right\}, \tag{22}$$

where the first term on the r.h.s. is evaluated at the lower boundary where the turbulent fluxes are specified. Note that in the last term of equation (22), since K^q is inside the integral, the z-dependence of the eddy diffusivity need not be specified. Rather, the integrated value over each element is all that is required.

The following boundary condition is chosen for the top of the surface layer (bottom of the lowest element):

$$B^q(h_s) = -g^q(\xi)\overline{q'w_0'} + K^q q_i\frac{\partial\phi_i(h_s)}{\partial z} = 0, \tag{23}$$

where $\overline{q'w_0'}$ is the turbulent flux of q at the top of the surface layer and $g(\xi)$ is a function of the surface layer stability parameter, ξ, which is given by the formula recommended by Barker and Baxter [22]. At the top boundary ($z = h_T$), the wind velocity is specified to be equal to the free atmosphere geostrophic wind. The potential temperature is also specified at the top boundary. After integrating and simplifying, the model equations may be stated as

$$\frac{h-h_s}{3}\dot{q}(h_s) = \frac{h-h_s}{3}Q^q(h_s) - \frac{h-h_s}{6}[\dot{q}(h) - Q^q(h)] + \left(\frac{\bar{K}^q}{h-h_s} + \frac{1}{6}\frac{dh}{dt}\right)[q(h) - q(h_s)] + g^q(\xi)\overline{q'w_0'} \tag{24}$$

and

$$\frac{h_T - h_s}{3}\dot{q}(h) = \frac{h_T - h_s}{3}Q^q(h) - \frac{h - h_s}{6}[\dot{q}(h_s) - Q^q(h_s)] - \frac{h_T - h}{6}[\dot{q}(h_T) - Q^q(h_T)]$$

$$- \frac{\bar{K}^q}{h - h_s}[q(h) - q(h_s)] + \frac{1}{3}\frac{dh}{dt}[q(h_T) - q(h_s)]. \quad (25)$$

A separate equation is written for the entrainment rate (dh/dt) following the procedure proposed by Nieuwstadt and Tennekes [23]; the details for application to our model are reported elsewhere [24]. Equations (24) and (25) show how naturally entrainment and the vertically integrated diffusion enter the model.

The temperature of the earth's surface is determined by using the surface energy budget of Brost and Wyngaard [9] that takes into account the downward i.r. radiation from the atmosphere, the upward i.r. radiation from the surface, upward sensible heat flux to the atmosphere and downward heat conduction into the soil. This budget treats conduction of heat into the soil by the force-restore method described by Deardorff [25]. Given the specific humidity, the downward flux of i.r. radiation may be specified by using the effective emissivity of Staley and Jurica [26].

The average eddy diffusivity over the boundary layer is determined from

$$\bar{K}^m = c_k\left(1 - \frac{\mathrm{Ri_B}}{\mathrm{Ri_{cr}}}\right)l^2 S, \quad (26)$$

where

$$\frac{1}{l} = \frac{1}{0.05h} + \frac{4.7}{kL}, \quad S^2 = \left(\frac{\partial u}{\partial z}\right)^2 + \left(\frac{\partial v}{\partial z}\right)^2 \quad (27)$$

and $c_k = 0.35$, $\mathrm{Ri_{cr}} = 1.0$ [10], $k = 0.4$ and the bulk Richardson number, $\mathrm{Ri_B}$, is related to the Monin-Obhukov stability parameter L, as given by Panofsky and Dutton [27]. We have taken the turbulent diffusivities for heat and momentum to be the same.

Equation (21), modified by equation (22), can then be written in matrix form as

$$\mathbf{A}^k\dot{\mathbf{q}}^k = \mathbf{A}^k\mathbf{Q}^k + \mathbf{C}^k\mathbf{q}^k, \quad (28)$$

from which the time tendencies are determined. The solution at step $k+1$ is then approximated from

$$\tilde{\mathbf{q}}^{k+1} = \mathbf{q}^k + \dot{\mathbf{q}}^k\Delta t. \quad (29)$$

Next, the time tendencies at step $k+1$ are estimated from

$$\tilde{\mathbf{A}}^{k+1}\dot{\mathbf{q}}^{k+1} = \tilde{\mathbf{A}}^{k+1}\tilde{Q}^{k+1} + \tilde{\mathbf{C}}^{k+1}\tilde{\mathbf{q}}^{k+1}, \quad (30)$$

where

$$\tilde{\mathbf{A}}^{k+1} = \mathbf{A}(\tilde{q}^{k+1}). \quad (31)$$

The final solution at step $k+1$ is calculated by using

$$\mathbf{q}^{k+1} = \mathbf{q}^k + [(1-\delta)\dot{\mathbf{q}}^k + \delta\dot{\mathbf{q}}^{k+1}]\Delta t. \quad (32)$$

The value of δ was taken to be 0.5.

Model Results

The model equations were used to simulate the stable nighttime boundary layer by beginning with a neutral steady-state condition and imposing a surface cooling rate of 1.0 K/h. The functions for the surface flux used for these simulations were

$$g^u(\xi) = 0.6 + 0.419\,e^{-12.0\xi} \quad \text{and} \quad g^v(\xi) = 0.45 + 2.80\,e^{-16.9\xi}. \quad (33)$$

The results at a time 12 h after the onset of surface cooling are presented in Table 1. It is apparent from this table that the model performs very well in comparison with the high-resolution, physically

more complete model of Wyngaard [8] and the bulk model of Zeman [10]. Additional stable simulation and adaptation of the model to the daytime boundary layer will be reported in a forthcoming report [24].

4. SUMMARY

We have described an adaptation of the finite element method to the problem of simulating the time-dependent behavior of the atmospheric boundary layer under conditions of surface heating or cooling and situations where the flow is subject to the dynamic influence of low terrain features. Features of the finite element method such as variable grid resolution, isoparametric elements, log-linear basis functions, time-dependent basis functions and vertically integrated properties can be exploited to advantage in such applications. Some techniques, such as the general application of the moving finite element method, require additional research into their potential advantage for boundary-layer modeling. For others, the advantages already are clear, such as the vertically integrated formulation which described gradients, entrainment and vertically integrated properties in a very natural way because of uniquenesses of the finite element method.

Acknowledgements—The authors wish to acknowledge J. Fast and L. Ly for use of their numerical results prior to publication. This research was supported in part by the Division of Atmospheric Science, National Science Foundation, under Grant ATM-8217210 and by the U.S. Air Force (Space Division). Partial support also was provided by the Auburn University at Montgomery Research Grant-in-Aid Program. Computational resources were provided by the National Center for Atmospheric Research, which is sponsored by the National Science Foundation.

REFERENCES

1. S. T. Chan, P. M. Gresho and R. L. Lee, Simulation of LNG vapour spread and dispersion by finite element methods. *Appl. math. Modelling* **4,** 335–344 (1980).
2. R. A. Pielke, *Mesoscale Meteorological Modeling*. Academic Press, Orlando, Fla (1984).
3. R. D. Russell and E. S. Takle, A numerical study of the effects of synoptic baroclinicity on stable boundary-layer evolution. *Bound.-Layer Met.* **31,** 385–418 (1985).
4. G. Therry and P. Lacarrere, Improving the eddy kinetic energy model for planetary boundary layer description. *Bound.-Layer Met.* **25,** 63–88 (1983).
5. L. P. Chang, E. S. Takle and R. L. Sani, Development of a two-dimensional finite-element PBL model and two preliminary model applications. *Mon. Weath. Rev.* **110,** 2025–2037 (1982).
6. J. Mailhot and R. Benoit, A finite-element model of the atmospheric boundary layer suitable for use with numerical weather prediction models. *J. atmos. Sci.* **19,** 2249–2266 (1982).
7. A. J. Thorpe and T. H. Guymer, The nocturnal jet. *Q. Jl R. met. Soc.* **103,** 633–653 (1977).
8. J. C. Wyngaard, Modeling the planetary boundary layer—extension to the stable case. *Bound.-Layer Met.* **9,** 441–460 (1975).
9. R. A. Brost and J. C. Wyngaard, A model study of the stably stratified planetary boundary layer. *J. atmos. Sci.* **35,** 1427–1440 (1978).
10. O. Zeman, Parameterization of the dynamics of stable boundary layers and nocturnal jets. *J. atmos. Sci.* **36,** 729–804 (1979).
11. J. L. Song, R. A. Pielke, M. Segal, R. W. Arritt and R. C. Kessler, A method to determine nonhydrostatic effects within subdomains in a mesoscale model. *J. atmos. Sci.* **42,** 2110–2120 (1985).
12. E. W. Peterson, P. A. Taylor, J. Hojstrup, N. O. Jensen, L. Kristensen and E. L. Petersen, Riso 1978: further investigations into the effects of local terrain irregularities on tower-measure wind profiles. *Bound.-Layer Met.* **19,** 303–313 (1980).
13 E. S. Takle and J. M. Leone Jr, Application of a log-linear element to a finite-element boundary layer flow model. *J. comput. Phys.* **53,** 514–523 (1984).
14. E. S. Takle and J. M. Leone Jr, A logarithmic-linear element for modeling geophysical boundary-layer flows. In *Finite Element Flow Analysis* (Edited by T. Kawai), pp. 859–865. Univ. of Tokyo Press, Tokyo (1982).
15. K. Miller and R. N. Miller, Moving finite elements 1. *SIAM Jl numer. Analysis* **18,** 1019–1032 (1981).
16. R. J. Gelinas, S. K. Doss and K. Miller, The moving finite element method. *J. comput. Phys.* **40,** 202–249 (1981).
17. S. Adjerid and J. E. Flaherty, A moving finite-element method with error estimations and refinement for one-dimensional time dependent partial differential equations. *SIAM Jl numer. Analysis* **23,** 778–796 (1986).
18. A. J. Wathen, Mesh-independent spectra in the moving finite element equation. *SIAM Jl numer. Analysis* **23,** 797–814 (1986).
19. N. Kim, Application of moving finite element method to the atmospheric boundary layer. M.S. Thesis, Iowa State Univ. Ames, Iowa (1984).
20. O. Zeman and H. Tennekes, Parameterization of the turbulent energy budget at the top of the daytime atmospheric boundary layer. *J. atmos. Sci.* **34,** 111–123 (1977).
21. J. Malcher and H. Kraus, Low-level jet phenomena described by an integrated dynamical PBL model. *Bound.-Layer Met.* **27,** 327–343 (1983).
22. E. H. Barker and T. L. Baxter, A note on the computation of atmospheric surface layer fluxes for use in numerical modeling. *J. appl. Met.* **14,** 620–622 (1975).

23. F. T. M. Nieuwstadt and H. Tennekes, A rate equation for the nocturnal boundary-layer height. *J. atmos. Sci.* **38,** 1418–1428 (1981).
24. R. D. Russell and E. S. Takle, a moving-grid finite-element model of the bulk properties of the atmospheric boundary layer. *Bound.-Layer Met.* Accepted for publication.
25. J. W. Deardorff, Efficient prediction of ground surface temperature and moisture, with inclusion of a layer of vegetation. *J. geophys. Res.* **83,** 1889–1903 (1978).
26. D. O. Staley and G. M. Jurica, Effective atmospheric emissivity under clear skies. *J. appl. Met.* **11,** 349–356 (1972).
27. H. A. Panofsky and J. A. Dutton, *Atmospheric Turbulence.* Wiley, New York (1984).